PI: Philip Goode

Earthshine Measurements of the Earth's Albedo

ABSTRACT:

The earth's climate depends on the net sunlight absorbed by the globe, which is quantified by the earth's albedo. A *global* and *absolutely calibrated* albedo can be determined by measuring the amount of sunlight reflected from the earth and, in turn, back to the earth, from the dark portion of the face of the moon (the "earthshine" or "ashen light"). Such data provide a critical complement to satellite data.

We have been measuring earthshine since December 1998, and have already demonstrated that the earthshine can be observed with sufficient precision to derive meaningful information about the earth's optical reflectivity. We have measured 20% seasonal variations in the earth's global albedo.

We propose to continue these observations from Big Bear Solar Observatory (BBSO), and expand them to a three-station network that will give us global coverage. The albedo data will also enable us to quantitatively assess the global effects of secular and seasonal variations, as well as those of transient phenomena such as a volcanic eruption, El Niño or La Niña. During the three year period proposed here (2001-2004), we will obtain a data base covering solar activity maximum and the declining phase of the current cycle, enabling us to determine the level of solar cycle dependence of the albedo. We propose to continue our modeling of earthshine by using scene models developed for the Earth Radiation Budget Experiment (ERBE). We have already found shortcomings in its averaging, which we propose to correct. Finally, we have begun seasonal observations of the earthshine spectra using the 60″ telescope on Mt. Palomar and its Echelle spectrograph. We propose to use earthshine spectral data to search for the degree of large-scale changes in the earth's atmosphere, its structure and composition.

PROJECT DESCRIPTION

I. Overview

For nearly two years, we have been measuring earthshine from Big Bear Solar Observatory (BBSO) to determine the earth's large-scale reflectivity. We have done this work with NASA support under the "Solar Influences on Global Change" program. Here, we propose to continue and expand this project.

The earth's climate is driven by the *net* sunlight reaching the climate system. The net depends on the sun's irradiance and earth's reflectivity. Thus, measuring the fraction of sunlight reflected by the earth strikes to the heart of NASA's Sun-Earth Connection Theme. The solar irradiance has been precisely measured for about twenty years, and over that period it has varied only slightly, with the irradiance being 0.1-0.2% greater during the maximum of the solar activity cycle, for a recent review see Lean (1997). The earth's reflectivity is not nearly so well-studied, but it does *not* seem to be nearly so stable, ESP, et al.(2000).

Knowing the earth's large-scale albedo, and its variation, is critical to determining the nature and trends of global climate change. About 30% of the incident sunlight is promptly reflected, so it never drives the climate system. Measurement of the albedo is complicated by its variation with the earth's aspect (land is more reflective than water), weather (cloud patterns), and seasons (snow and ice cover). Earthshine measurements would be also sensitive to changes in the net deposit arising from volcanic eruptions, like Mt. Pinatubo, and regional changes in albedo arising from large-scale phenomena, like El Niño and La Niña events. The period of the observations proposed here runs from 2001-2004, which when combined with our on-going observations, would give data covering 1999-2004 – the time solar activity goes through its maximum and subsequently declines down to its minimum – allowing us to investigate whether the earth's albedo depends on the phase of the solar cycle.

The albedo is determined most directly by satellite observations (Gibson, et al. 1990, Stephens, Campbell and VanderHaar 1981, Rossow and Lacis 1990). However, satellites in low-earth orbit view only a small fraction of the earth's surface at once, so that many observations must be combined to obtain global-scale information on the albedo. Moreover, it is a major technical and logistical challenge to keep calibrated photometers continuously in orbit on decadal timescales.

The earthshine, or "ashen light", is the glow of the "dark" part of the lunar disk visible to a nighttime observer, see Fig. 1. It is sunlight reflected from the earth and retroflected from the lunar surface, and so offers an alternative route to studying the earth's reflectance. Earthshine data are complementary to satellite data in that the coverage is instantaneous and global in scale. For instance, at the quarter-moon, there is a three-quarter earthshine. Thus, at any moment one has a snapshot of the albedo of the three-quarters of the hemisphere of the earth that is sunlit. That coverage represents the area of the earth for which we measure the albedo of the earth on a typical night's observing from BBSO. We intend that our earthshine observations will be long term, and they therefore can link data from, say, one satellite to its successors.

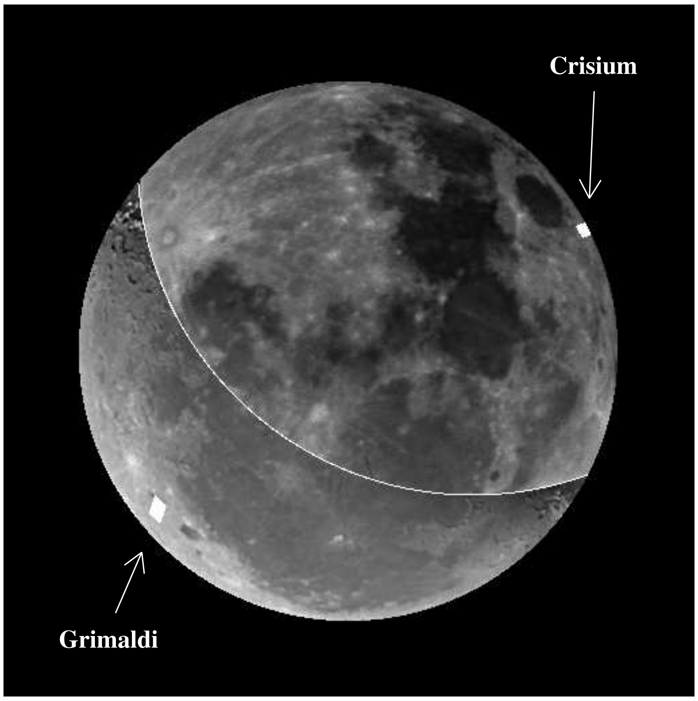

Fig. 1. Processed image of the moon from May 29, 2000 at lunar phase 125°.6 (declining phase). As seen from the earth, the lower part is illuminated by obliquely reflected sunshine (so-called "moonshine"), so that shadows and crater rims are clearly visible. The upper part is illuminated in the retroflected earthshine, and it shows flatter features. This difference results in some features, like the mare or "seas", persisting across the terminator, while others do not.

For a quarter century, beginning in the 1920s, Danjon and his followers (Danjon 1928, Danjon 1954, Dubois 1942 and Rougier 1933) performed regular earthshine observations from France. We have reinvigorated and modernized this nearly forgotten way of measuring the earth's albedo. Danjon used a "cat's-eye" photometer to produce a double image of the moon, allowing the visual comparison of the intensities of two well-defined regions of the lunar surface−−one in sunlight and the other in the earthshine−−at various lunar phases. Using the "cat's-eye" mechanism, he stopped down the light from the sunlit portion to match the brightness of the ashen portion. This differential measurement removed many of the uncertainties associated with varying atmospheric absorption and the solar constant, allowing Danjon to achieve an estimated uncertainty of roughly 5%. Our measurements are nearly an order of magnitude more precise, not simply because we have better cameras, but we have also solved the problem of the uncertainty in the scattering from the moon as a function of the phase of the moon (see Fig. 3 in §II.1). Our terrestrial measurements of the earth's albedo have a precision comparable to that quoted for satellite results (Gibson, et al. 1990, Stephens, Campbell and VanderHaar 1981, Rossow and Lacis 1990).

Under NASA support, we have the following publications and presentations:

Publications:

"Earthshine and the Earth's Reflectance", 2000, Goode, P.R., Qiu, J., Yurchyshyn, V., Hickey, J., Koonin, S.E., Brown, T., Chu, M.C. and Kolbe, E., Science, submitted.

"The Earth's Albedo from Earthshine", 2000, Qiu, J., Goode, P.R., Yurchyshyn, V., Hickey, J., Koonin, S.E., Brown, T., Chu, M.C. and Kolbe, JGR, in preparation.

"Large-Scale Variations in the Earth's Atmospheric Structure from Spectral Observations of Earthshine", 2000, Koonin, S.E., Brown, T., Goode, P.R., Qiu, J., Yurchyshyn, V., Hickey, J., Brown, T., Chu, M.C. and Kolbe, E., JGR, in preparation.

Presentations:

"Earth's Albedo from Earthshine, 2000, Goode, P.R., Qiu, J., Yurchyshyn, V., Hickey, J., Koonin, S.E., Brown, T., Chu, M.C. and Kolbe, E., Living With a Star Meeting, Tucson, March 2000.

"Earthshine and the Earth's Albedo", 2000, Goode, P.R., Qiu, J., Yurchyshyn, V., Hickey, J., Koonin, S.E., Brown, T., Chu, M.C. and Kolbe, E., AAS/SPD Meeting, June 2000.

"The Earth's Reflectivity from Earthshine ", 2000, Goode, P.R., Qiu, J., Yurchyshyn, V., Hickey, J., Koonin, S.E., Brown, T., Chu, M.C. and Kolbe, E., Euroconference on "The Solar Cycle and Terrestrial Climate(SOLSPA2000)", talk and paper.

II. The Earthshine Project

We have been measuring the earthshine from Big Bear Solar Observatory (BBSO) since December 1998. From California, we see the moon reflecting sunlight from Asia and the western Pacific in our evening – before midnight – which is during the moon's rising phase, and from Africa, Europe, the Atlantic and the eastern New World in our morning – after local midnight – which is during the moon's declining phase. We have precisely measured the brightness of the moon, as a function of lunar phase, which enables us to determine the nightly averaged reflectance of the earth to about 1% on most nights. Averaging our data, we see 20% seasonal changes, with the earth being brightest in the spring, ESP, et al. (2000). This corresponds to a change in the earth's albedo, A, of about 0.06.

II.1. The Earthshine Observations and Determination of Albedo

Our earthshine coronagraph is a 6-inch refractive telescope with a cooled AP-7 512×512 CCD camera, as shown in Fig. 2. We mask the bright portion of the lunar disk with a neutral density filter with a transmission of approximately 10^{-5}, and correct the measured earthshine intensity for the effects of moonshine scattered in the atmosphere and optical train. The nightly observations consist of 0.5-3.0 min earthshine measurements taken once every five minutes, with 0.1-5.0 s moonshine observations interspersed. Dark current and flat-field images are taken regularly.

Because the earth's phase as seen from the moon is supplementary to that of the moon seen from the earth (i.e., the earth is nearly "full" when the moon is a thin crescent), the instantaneous intensity of the earthshine can sample almost half of the earth. Earthshine is most conveniently determined by observing the relative intensities, $I_{a,b}$, of two nearly diametrically opposite fiducial lunar highland regions near the edge of the lunar disk, one (a) in the earthshine, the other (b) in the sunlight, or so-called "moonshine". The regions we used are indicated in Fig. 1. They are in the lunar highlands near Crisium and Grimaldi. Each covers nearly 0.1% of the lunar disk, or about 100 pixels. If we define the

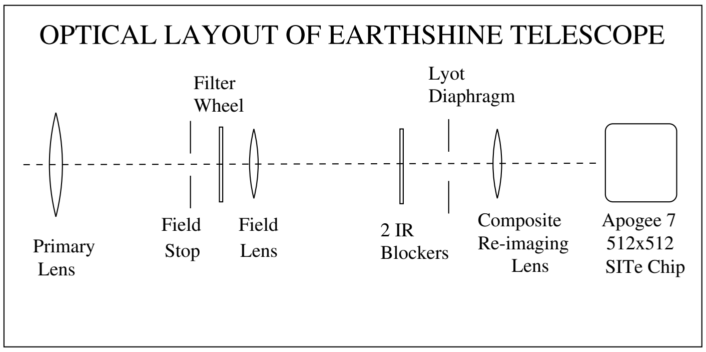

Fig. 2. The optical set-up of the BBSO earthshine coronagraph.

effective albedo of the earth, A^*, as the albedo of a Lambert (perfectly diffusing) sphere that would have the same reflectivity as the true earth, then

$$A^* = \frac{3}{2}\frac{f_b}{f_L}[\frac{R_{em}^2}{R_e^2}]^2\frac{p_b}{p_a f_a}\frac{I_a}{I_b}. \tag{1}$$

Here, θ is the lunar phase (θ is nearly $-\pi$ at the new moon, increases to near $\theta = 0$ at mid-month, and is nearly $\theta = \pi$ at the end of the lunar month), $f_b(\theta)$ is the phase function of region b, $\beta \approx \pi - \theta$ is the earth's phase angle, and $f_L(\beta) = [(\pi- \mid \beta \mid) \cos\beta + \sin \mid \beta \mid]/\pi$ is the Lambert phase function. (All phase functions are defined so that $f(0)$=1.) The lunar phase function, $f_a(\gamma)$, arises from the near retroflection of the earthshine by the moon, where γ ($\leq 1°$) is the angle between the incident and nearly retroflected earthshine from region a. R_{em} and R_e are the earth-moon distance and radius of the earth, respectively. Although we quote a geocentric formula for simplicity here, all of our analyses are performed using a more precise expression involving topocentric quantities.

Our differential measurement of earthshine removes many of the uncertainties associated with varying atmospheric absorption and solar intensity. Lunar images around a lunar eclipse determine the ratio of the geometrical albedos of the two fiducial regions, $\frac{p_b}{p_a}$, while photometric observations of the sunlight crescent during many lunar cycles determine the phase functions, f_a and f_b.

To fully account for the effect of atmospheric extinction, observations of both the earthshine and the moonshine are made as the airmass varies each night. The true intensities to be used in Eqn. (1) are greater than the observed intensities by a factor of $e^{\alpha z}$ (Beer, et al. 1991). The local airmass, z, is the cosecant of the elevation angle for observations near the zenith. Near the horizon, the curvature of the earth requires that we use tabulated values (Kondratev 1973). The atmospheric extinction coefficient, $\alpha \sim 0.15$, is determined for the earthshine and moonshine by fitting each night's observations.

To determine the earth's reflectance from the earthshine, we must know the lunar phase function – the scattering of sunshine from the fiducial regions as a function of the phase of the moon. The lunar phase function is determined from the moonshine. The problem is that even raw *moonshine* data near the quarter moon show as much as a 5% variation from month-to-month at the same lunar phase. To address this problem, we observed the moonshine and earthshine for each night during 1999 that it was not cloudy

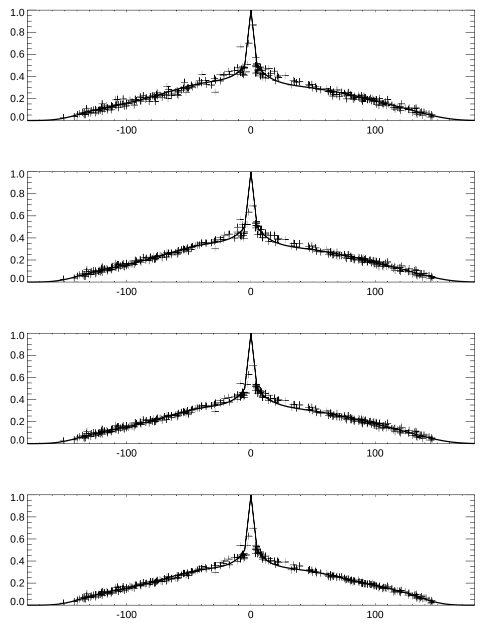

Fig. 3. Lunar phase function plots from the raw data, and from data after each step of correction. The y-axis is the intensity light scattered from the fiducial regions relative to that at the full moon. The peak near small phase angles arises from a coherent backscatter from the lunar soil, Flatté, et al. (1991). This is the so-called "opposition effect". Negative phase angles refer to the rising phase of the moon, and scattering from the highlands near Crisium. Positive phase angles refer to the declining phase and scattering from the highlands near Grimaldi. These regions are indicated in Fig. 1.

in Big Bear. We also continue to observe the moonshine every night the phase angle is small. From that, we presently have data from 286 nights (and counting). After some thought, we found we could solve this long-standing problem by making three successive, physically required, linear corrections to the lunar phase data, see Fig. 3. We used the crescent of the moon as a standard to correct for nightly intensity variations – see the differences between the top panel and second panel in Fig. 3. This correction is more significant for the evening data (lunar phase <0) because we are mostly observing the moon in the western sky over Los Angeles and the Pacific Ocean, which is more subject to local atmospheric variations. Next, we corrected for the declination of the moon which is different from month-to-month for the same lunar phase (e.g., there is not a total eclipse of the moon each month) – see the changes between the second and third panels. This correction is most important near the full moon where the relative position of the moon matters most. Last, we corrected for the libration of the moon. After applying these three physically required corrections, the aforementioned 5% variation is reduced by an order of magnitude, allowing us to measure the nightly effective albedo to about 1% on most nights. Again, these levels are comparable to those quoted for satellite albedo data (Gibson, et al. 1990, Stephens, Campbell and VanderHaar 1981, Rossow and Lacis 1990).

In Fig. 4, we compare our nightly averaged observed results (left panel) to simulated

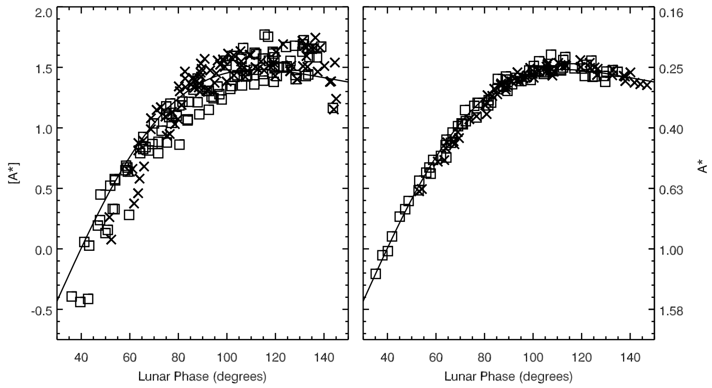

Fig. 4. Plot of $[A^*]$ and A^* against the absolute value of the lunar phase for the 137 nights between Jaunary 1999 and July 2000 for which we had clear skies, and there also was simultaneous satellite cloud cover data for the parts of the earth illuminated by the earthshine. The left panel shows observational results and the right one shows simulations. Each data point in the left panel represents a nightly averaged $[A^*]$. The x's indicate morning observations (lunar phase > 0), and empty boxes indicate evening observations (lunar phase < 0). We emphasize that error bars would be within the symbols. Each simulation point covers a night for which there is observational data and cloud cover data. Each of the latter points represents the average over the times of the observations for that night. To help compare, the same solid curve is shown in both panels. It is a 4^{th} degree polynomial fit to the *simulations* for all nights and all phase angles. Note that the smaller the value of $[A^*]$, the shinier the earth.

results (right panel) using satellite data for cloud cover, and snow and ice cover for the same times and areas of the earth. In modeling the reflectance properties of the earth, we used scene models developed for the Earth Radiation Budget Experiment (ERBE) observations (Suttles, et al. 1988). These scene models give local reflectance as a function of illumination and reflection directions, snow and ice cover, fractional cloud cover, and surface type. For the snow/ice cover, we used simulations from the Canadian Center for Climate Modeling and Analysis (`http://www.cccma.bc.ec.gc.ca`). The model gives the monthly mean snow/ice cover for each grid cell ($2.5° \times 2.5°$). The cloud cover data input to the model came from Weather Service International (WSI-INTELLICAST: `http://www.intellicast.com/`) which provides real-time weather data.

The left panel of Fig. 4 shows the effective albedo from our data expressed in astronomical magnitudes, $[A^*] = -2.5 \log A^*$, as determined from all of our earthshine observations on clear nights. This standard astronomical definition implies that the larger $[A^*]$ is, the smaller the albedo. Note that a 1% change in A^* corresponds to a $0^m.01$ change in $[A^*]$. Each data point represents a nightly averaged $[A^*]$ value. The nightly $[A^*]$ is relatively flat for larger phase angles ($\theta \sim \pm 120°$), but it decreases sharply toward the full moon. Hence, the earth is relatively more reflective at grazing angles (glint). Note that there are no reliable observations for phase angles below 40° or above 140° because of scattered moonshine, and because of short observing nights, respectively.

The mean values of the $[A^*]$'s in both the right and left panels show the same behavior with lunar phase. Furthermore, there are no apparent differences between $[A^*]$'s determined from BBSO morning observations (lunar phase > 0) and those from evening observations (lunar phase < 0). However, independent of lunar phase, the observational results show about twice the spread about the mean than the simulations. The changing cloud cover induces a $\sim 5\%$ night-to-night variation in the observed A^*, even for the larger phase angles where the data are most reliable and the earth is close to a Lambertian surface (i.e., A^* depends only weakly on the lunar phase). The variations in the left panel of Fig. 4, for either morning or evening observations near the larger phase angles, are $\sim$20%. In §III.1, we discuss our understanding of the origin of the difference in spread between the two panels, and how we propose to test and advance our understanding.

To determine the annual, average Bond Albedo (the fraction of all light that is reflected), one needs to integrate the observed or simulated A^*'s over all phases, using

$$A = \frac{2}{3} \int_{-\pi}^{\pi} d\theta f_L(\theta) A^*(\theta) \sin\theta. \tag{2}$$

For the simulations, the integration is straightforward. We simply calculate A^* for all lunar phases, not only those at which we have observational data (as in the right panel of Fig. 4). Fitting a curve through these points to define $A^*(\theta)$ and integrating Eqn. (2), we obtain $A = 0.294 \pm 0.002$ for our simulations to date. We have the same result irrespective of whether we focus on the morning or evening simulations. For the observational data, we need to extend the fits out to lunar phase angles near 180°, as well as to angles below 40°. We do this by constrained least squares fits in which smooth changes are assumed in the phase function with phase. The calculations convert 1σ variances in the data to a 1σ variance in the fitted curve. This method is used, widely and successfully, in helioseismology. For a review of the method and its utility, see Goode (1995). We tested the method by using it to extend simulations between 40° and 140°, as in Fig. 4, and we determined $A = 0.293$. The fitted curve and A are indistinguishable from their counterparts using the simulated data covering the entire range from 0° to 180°. With this in mind, we apply the method to our data in precisely the same way and find $A = 0.297 \pm 0.005$ for the two-thirds of the earth that we observe – this result is quite consistent with the result from the simulations. During the rising phase of the moon ($\sim$Asia and the western Pacific), we find 0.295 ± 0.007 for 104 nights; and we find 0.297 ± 0.007 for the 94 nights in the morning observations which occur during the lunar declining phase ($\sim$Europe/Africa/Atlantic/eastern New World). The quoted errors arise from the fit, including the formal uncertainty from the extension. The larger error bars in the observational data primarily reflect the broader spread seen in the left panel of Fig. 4. The values of A quoted here are sufficiently precise to detect the secular, seasonal and year-to-year variations in the earth's albedo.

III Proposed Work

We have found intriguing and significant results in our first eighteen months of earthshine observations. Motivated by this we propose:

1) to continue secular and seasonal observations of the earthshine to look for long-term effects.

2) to create a global earthshine network. We have made agreements with two well-respected observatories – the Crimean Astrophysical Observatory (CrAO) and Yunnan Observatory (YO) – to join with us, so we will have continuous, global coverage. Further, the network would roughly treble our data rate.

3) to determine, at the least, an upper limit on the solar cycle variability of the albedo using data in hand, plus that to come over the peak and declining phase of the current cycle (which encompasses the period of the work proposed).

4) to continue the corresponding simulations using satellite cloud cover data, including the use of alternative scene models and other sources of cloud cover data.

5) to make winter and summer observations of earthshine spectra from the 60″ telescope at Mt. Palomar in order to determine the large-scale variations of the earth's atmosphere, including the amount of water vapor and effective temperature of O_2 and H_2O.

Earthshine measurements provide a calibration which will be especially useful in determining large-scale trends in weather and climate. Another motivation, comes from the controversial result of Svensmark and Friis-Christensen (1997) who used satellite data to infer that the earth is 3-4% cloudier at activity minimum. If this were true, it would have appreciable affects on the albedo. Our albedo measurements over the declining phase of the present solar cycle would detect such a variation, if present.

III.1 Secular and Seasonal Earthshine

Each night we observe, we will determine an effective albedo. We will simulate all nights. For the nights we observe, and there is corresponding satellite cloud cover data, we will compare the simulations with the observations. To illustrate this, in Fig. 5 we show the observational and model results for two nights – one "evening" and one "morning". The top panels show that a significant part of the earth contributes to the earthshine during the observations. For larger lunar phases, more of the earth contributes instantaneously to the earthshine, but the length of the observations is reduced. For smaller lunar phases, less of the earth contributes to the earthshine at any moment, but there is a relatively longer observing night. Hence, somewhat more than a third of the earth is covered during a given night, roughly independent of phase. The middle panel in Fig. 5 shows the effective albedo as a function of time (note that the time is plotted in reverse chronological order). The solid curve connecting the diamonds shows the variation of the calculated effective albedo, and the solid boxes are the observed effective albedo. The results in Fig. 5 come from near to the quarter moon – one waxing and one waning. The observations are consistent with the model simulation from the cloud cover data for 24 March 1999, one of the nights for which the agreement is quite good. On 31 October 1999, a more typical night, only the forms of the curves are the same. The overall difference is about 5% in the effective albedo

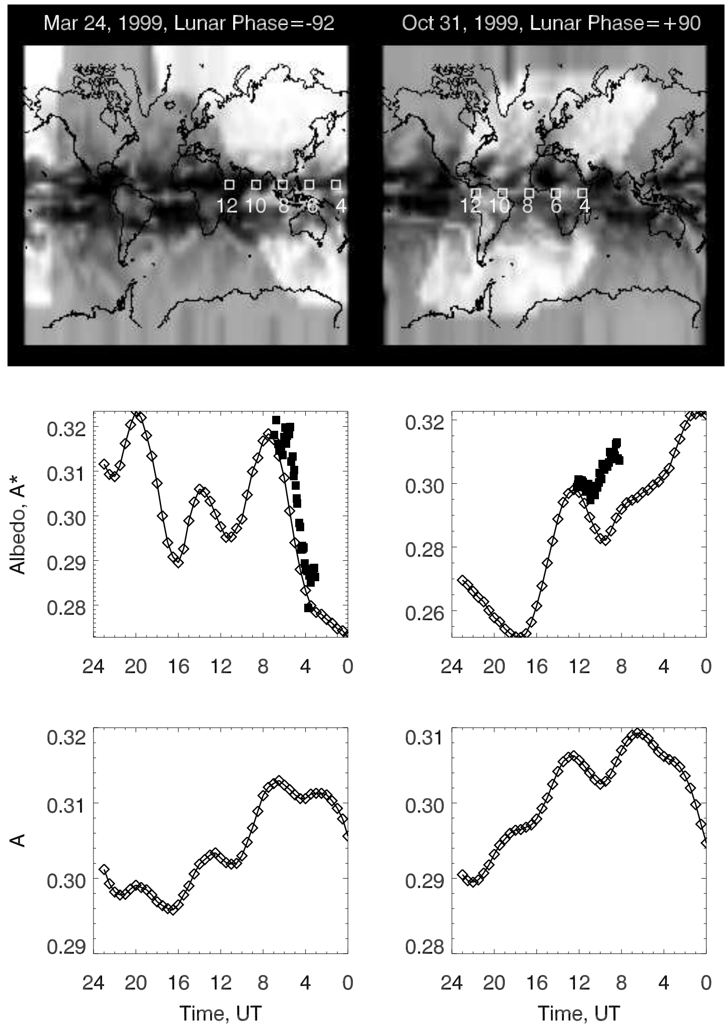

Fig. 5. The top panels show the bright, sunlit parts of the earth visible during the observations, overlaid on a Mercator projection map of the earth. A second overlay, in gray-scale, is the satellite cloud cover with brighter areas indicating greater cloud cover. For 31 October 1999, note that the northernmost regions are not sunlit, and the southernmost regions do not contribute to earthshine because the moon is fairly far north in the sky. The boxes indicate the areas of maximal contribution to the earthshine at the UT time shown. The middle panels show the observed (solid boxes) and calculated (diamonds) A^*'s for March 24, 1999 and 31 October 1999. The bottom panels show the simulated, visible light Bond albedo each half-hour for the sunlit area of the earth.

(or about 0.015 absolute). The bottom panel shows the variation of the total visible light albedo, calculated through the twenty-four hour days, on the left and right of Fig. 5.

At high geographical latitudes ($> 45°$), the fractional cloud cover is fairly high, so that the short timescale variations in albedo are mostly defined by irregularities in the fractional cloud cover at low latitudes. One sees, for instance, in the middle left panel of Fig. 5, that the observed and calculated maxima in A^* at 7:00 UT are due to a relative cloud excess over the Far East, while the calculated local minimum in A^* at 11:00 UT arises from the cloudless area above India and the Arabian Sea. In the left middle panel, we see a roughly 10% change in A^* through the period of the observations. The offset between the observed and calculated effective albedos evident in the middle right panel is a general result due to the observed night-to-night variations being greater than those in the simulations. What is the origin of the larger variation in the observations, as seen in Fig. 4? The A's from data and simulations agree quite well. Decomposing the data by season sheds light on the origin of the spread.

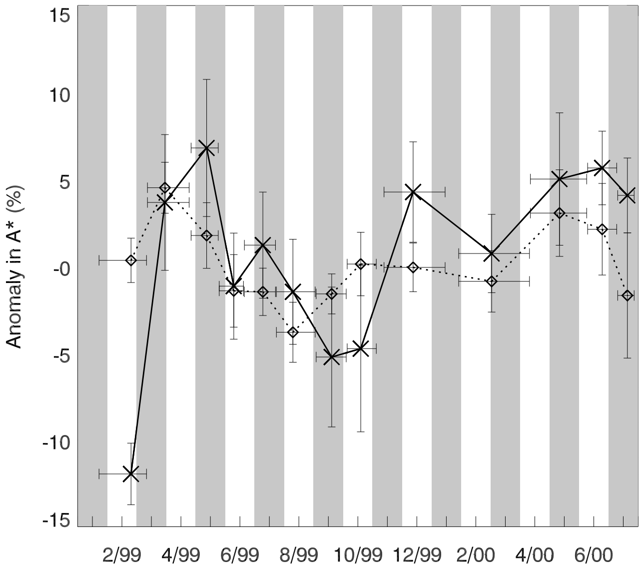

Fig. 6. Seasonal anomalies in the effective albedo, A^*. The 137 nights, from January 1999 through July 2000, for which we have both observations and contemporaneous satellite cloud cover data have been averaged in 11 consecutive groups. The X's indicate the observational data with the vertical errors being the standard deviation of the mean of the data. The size of the latter stems from the large night-to-night variations in the cloud cover, rather than from uncertainties in the observations. The horizontal error bars indicate the temporal span of the binned data. The diamonds indicate the model results using contemporaneous cloud cover data.

Our observations have determined both the variation of the instantaneous A^* during each single night, and the variation of the nightly average A^* through the seasons. We further emphasize that the variations in A^* with respect to the mean, depend strongly on the season, but quite weakly on the lunar declination. This observational result is directly confirmed from modeling. To illustrate the seasonal dependence, in Fig. 6 we plot the seasonal variation of the albedo to date. As $[A^*]$ is a strong function of lunar phase, we consider the anomaly of each nightly average relative to the best-fit mean. *By removing a mean from the variations, we remove the sensitivity to ambiguities in the ratio of moon's geometric albedos,* $\frac{p_b}{p_a}$*, and the lunar phase function,* f_b. The anomalies are shown as percent changes in the effective albedo. The anomalies carry the information about weather, climate and surface type. One can see a clear seasonal trend, with the earth being brightest in the spring. The earth is also cloudiest then. We see the seasonal trends in Fig. 6 in spite of the fact that the night-to-night variations are large. We emphasize that the large vertical "error" bars arise from the large night-to-night variations in the cloud cover, rather than any errors in the data. With all of this, we see a roughly 20% seasonal variation in albedo. The greatest discrepancy between the observations and simulations in Fig. 6 is in the first bin. Careful inspection of the simulations and observations which contribute to that bin reveal nothing special but the systematic difference between observations and simulations. With or without the first bin, it is Fig. 6 which points us toward interpreting the greater spread in the $[A^*]$'s in the left panel of Fig. 4 as likely being due to an inadequate treatment of cloud cover in the model.

In Fig. 6, we also compare our observed results to simulated results using satellite data for cloud cover, and snow and ice cover for the same times and areas of the earth. We see from the figure that the results are correlated. We emphasize that the seasonal variations in the calculations are about half those in the data, and the differences are greatest at the extremes. The weaker variation in the model would seem to result from the tendency of the model to smooth real terrestrial variations. Nonetheless, the correlation gives additional confidence in satellite measurements of albedo, and vice versa.

We presume the muted seasonal variations arise from a too coarse binning of the albedo in the scene models. In particular, for the cloud cover, the ERBE simulations have four bins – 0-5%, 5-50%, 50-95% and 95-100% cloud cover. This seems to be sufficient for an annual global average, but not for seasonal changes. We propose to probe the seasonal dependence with more data which we'd use, in part, to calibrate cloud cover satellite data and reduce the shortcomings in the scene models (or use better models where available). *We need much more data because we need to determine a precise albedo, and its seasonal and longer term variations, in the face of large night-to-night variations in the earth's effective albedo.* This point is made, from a different perspective, in the left panels of Fig. 5 for which the observations and simulations both show a 10% change in the effective albedo over a couple of hours.

We have demonstrated that the earthshine can be observed with sufficient precision to derive meaningful information about the earth's optical reflectivity. However, our observational results cover only the part of the earth we detect from California. To measure the earthshine for the whole earth, we require a network. We propose to build such a network, and we explain that three stations are sufficient. Tripling the data rate will provide invaluable additional data.

III.2 Earthshine Network

Our proposed earthshine network will have three sites. In addition to BBSO (116° 54.9′ W and 34° 15.2′ N at 2067 m), we have Yunnan Observatory (102° 47.3′ E and 25° 1.5′ N at 1940 m) and the Crimean Astrophysical Observatory (34° 1′ E and 44° 32′ N at 600 m). All three observatories have experienced staffs. Three stations are sufficient to cover the earth. The two new stations would see earthshine from the 2/3 of the world we can't see from California on any particular night, while providing more complete coverage of the parts of the world BBSO sees, Fig. 7. For instance, during the rising phase of the moon, the Crimean Observatory would see the Atlantic and New World, while BBSO would see the western Pacific and Asia, and Yunnan would see the Atlantic/Europe/Africa. Fig. 7 illustrates that on clear nights, one can measure the earthshine for the whole earth – even near the new moon where the observing nights are short because the angle between the moon and sun is small for the observer. On such nights, one might only observe for a total of six hours (two from each of the three stations), but at each moment during the observations, one is measuring the earthshine from nearly a whole hemisphere. For smaller lunar phases, the observing period from each station would be longer, while the part of earth in the earthshine, at any moment, would be smaller, but the net effect would be that each station would cover somewhat more than a third of the earth. Thus, even though the network is not operating twenty-four hours a day, one has daily, global coverage of the earthshine, from which we propose to determine a daily whole earth effective albedo. Using cloud cover data, like that illustrated in the top panel of Fig. 5, we also propose to calculate a corresponding whole earth albedo.

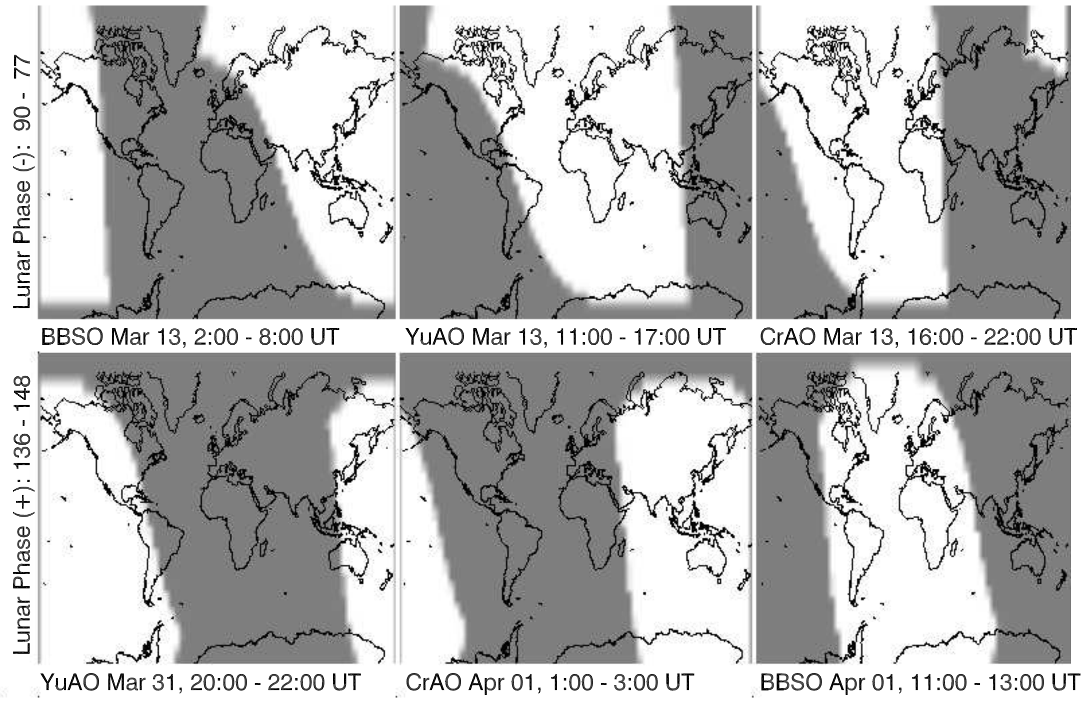

Fig. 7. The top panels show the bright, sunlit parts of the earth that would have been visible in the earthshine at a lunar phase varying between -90° and -77° on March 13, 2000 during four hours of observations from each site. The second row of panels is for two hours of observations from each site at a lunar phase between +136° and +148° on April 1, 2000. The earth is shown on a Mercator projection map. It is clear that the full earth is covered for both lunar phases.

The network also brings more subtle benefits, such as allowing us to determine $[A^*]$ vs. lunar phase separately for all nights that each observatory looks west and each looks east. A constant off-set between the two would point to systematic error in $\frac{p_b}{p_a}$. The ratio, $\frac{p_b}{p_a}$, is determined from total eclipse data (lunar phase ≈ 0). We have data from one eclipse covering about eight hours, from which we determined the intensity at zero airmass and the opposition effect. A network will allow us to measure each total lunar eclipse, while on the same night measuring the lunar phase function for small lunar phases from the other network sites – data that can only be obtained on nights during which there is a total eclipse somewhere. This proposal covers the period 2001-2004. During that period, there will be five total eclipses of the moon – each visible from at least one of our network sites. The other sites will measure the phase function at very small lunar phases. Thus, the network will greatly sharpen our determination of the lunar phase function, especially the value of $\frac{p_b}{p_a}$ and the structure of the opposition peak near 0° phase angle, where we now have relatively few data points (see Fig. 3). We also propose to use satellite data, like that from Clementine, to pin down the opposition effect. Using our improved phase function, we will re-analyze all earthshine taken since the beginning of the project. We also plan to use our phase function to re-analyze the earthshine data of Danjon and followers in an effort to tie back to the historical records.

The agreement with our partner observatories is that we will provide the camera/computer/optics, etc. for the earthshine telescopes, and they will each provide an observer, telescope tube, dome, etc. The two new earthshine telescopes will be built, tested, calibrated side-by-side in BBSO, and then shipped to our partners. Next, we will help assemble and bring into operation the partner telescopes. BBSO already has successful experience in building a daytime network under the same principles. The daytime network studies solar flares for space weather studies (visit our website www.bbso.njit.edu).

We would be able to have the earthshine network in place within three months of funding. With this network, we propose to accurately measure the albedo of the earth – at a level that is climatologically significant. Further, we propose to use our data to properly calibrate cloud cover satellite data and reduce the shortcomings in the scene models.

III.3 Spectral Studies from Mt. Palomar

The earthshine spectra carry detailed information about the global properties of earth's atmosphere. We would like to know how the atmosphere's composition and temperature change with the seasons, and if there are long term changes. Earthshine has traveled through the atmosphere three times (twice globally and once locally), during which molecular absorption spectra are formed. The local absorption can be removed by comparison with the moonshine spectrum. A careful study of the earthshine spectrum yielding an accurate measurement of the molecular parameters can help to determine global atmospheric quantities, like temperature, water vapor content, cloud optical depth and pressure.

To observe the earthshine requires a large aperture telescope equipped with a very precise spectrograph. Fortunately, the 60″ telescope on Mt. Palomar has a high quality Echelle spectrograph, and we have been able to make observations of both the moonshine and earthshine spectra with it. Our initial goal was to make two sets of broad spectral observations, about six months apart, to look for spectral changes. We had two runs in September, 1999 and two in March, 2000. These four runs comprise fifteen nights; two were evening runs (observations before local midnight) when the lunar phase was negative, and the other two were morning runs (observations after the local midnight) when the lunar phase was positive. This way, we have maximal coverage of the earth's atmosphere (both ∼Asia/western Pacific and ∼the Atlantic/Africa/Europe). The moonshine, earthshine, and sky spectra were taken consecutively at varying airmass. Some illustrative results are shown in Fig. 8.

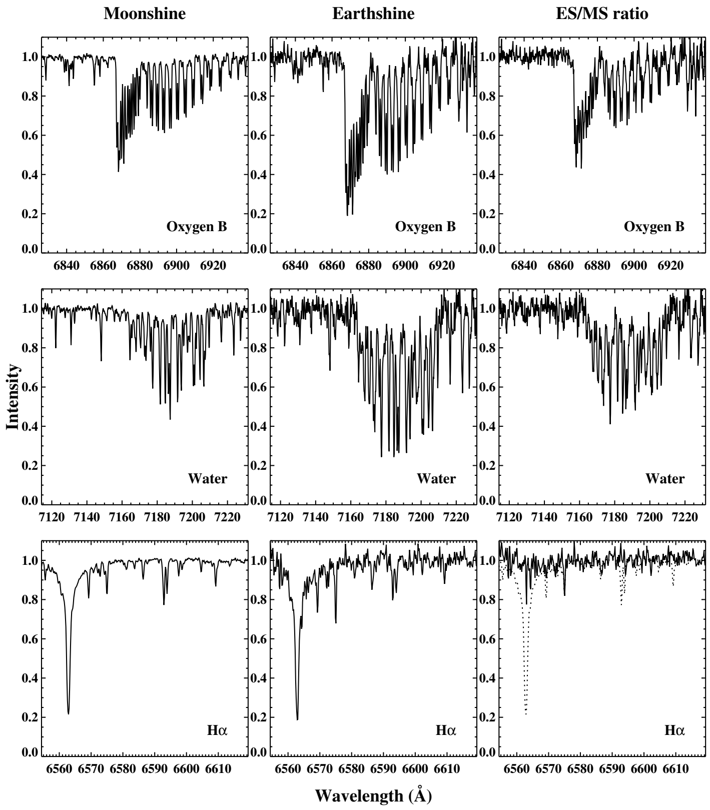

Fig. 8. The relative intensity of terrestrial oxygen and water, as well as lines in the spectral region of Hα, are shown, from left to right, in moonshine, earthshine, and the ratio of the earthshine to the moonshine. The dotted lines in the lower right panel illustrate the location of Hα and some other solar lines. The solar lines are clearly absent in ES/MS

In our analysis of these spectra to date, we focused on several spectral bands. Among these are the Oxygen B band ($14450 - 14560\ \mathrm{cm}^{-1}$) with groups of doublets from electronic-vibrational transitions, the water band at $13620 - 13960\ \mathrm{cm}^{-1}$ with groups of lines from rotational transitions, and the Hα band. The first two features are typical terrestrial molecular lines, from which we obtain the information about the earth's atmosphere, while the fourth line is a solar feature, which should be identical in the moonshine and earthshine spectra. In particular, the Hα line is taken as a check of the spectral calibration.

These spectra were carefully calibrated. The calibration procedures include: bias removal, flatfielding, dispersion calibration, sky subtraction, and normalization to the continuum.

Fig. 8 shows that the solar features in the Hα band (including other nearby solar lines which are mostly Fe) are absent in the ratio spectrum, while atmospheric features remain in the ratio spectra of the molecular lines. The clean removal of the solar lines implies that the spectral calibration is done correctly. Further, the ratio spectra at different airmasses do not differ, implying that the local atmospheric attenuation is also correctly removed. Thus, the spectra in the right panels are from the pure earthshine.

A least square non-linear iterative fitting algorithm has been developed to fit the multi-component Lorentzian profile, which is used to describe the observed and processed spectra. From the fitting, physical parameters of the absorption spectrum (line strength, line width, and line position) are obtained, and are compared with the HITRAN atmospheric molecular spectrum database to derive the effective temperature and molecular column density of the global atmosphere.

We analyzed the spectra from the four best observing nights, and the preliminary results show that the effective temperature of the atmosphere in March is about 10 K lower than in September. However, to draw solid conclusions, we need more observations at different seasons, and they are already scheduled. We will analyze much more of the spectra than shown in Fig. 8. We plan for alternating winter and summer observations at Palomar. Obviously, detailed modeling of the earth's reflectivity (e.g., cloud heights) will be needed to properly interpret these data.

IV. Budget and Operational Plan

We are requesting funds to support a postdoctoral associate and an observer. In addition, during the first year, we request \$35 K to purchase the hardware for our two network stations. This includes \$23 K for two cameras, computers and software, and \$12 K for two sets of optics, filters, mounts and parts. The cameras will be the same as the one we are currently using for our observations at BBSO. It is a 16-bit, 512x512 visible light CCD camera system from Apogee Systems (AP-7). The AP-7 has shown itself to be stable for the extremely long exposure times necessary for earthshine observations.

The current postdoctoral position is split between Jiong Qiu and Vasyl Yurchyshyn. They have close, personal ties with Yunnan Observatory and the Crimean Observatory, respectively. Jeff Hickey, who is the observer, has assembled the current system. Hickey, Qiu and Yurchyshyn are all veteran earthshine observers. The team now has extensive experience in all aspects of determining albedo from the earthshine, including instrumentation, data collection, and careful reduction and interpretation of it, as well as modeling the results, such as cloud cover from satellite data. For the network, Hickey will assemble and test the network telescopes in Big Bear, and travel to Yunnan (with Qiu) and to the Crimea (with Yurchyshyn) to put in place the partner telescopes. These two person teams will also train the remote observers. This approach is similar to that used for our already successful global Hα network.

Phil Goode, Steve Koonin and Yuk Yung will be donating time to the earthshine project. Goode is a professor of physics at NJIT, and he is the Director of BBSO. Koonin is Vice-President and Provost at Caltech, as well as being a professor of theoretical physics. Goode and Koonin have been leading the earthshine project to date. Yung is a professor of planetary sciences at Caltech. With his expertise in atmospheric physics and chemistry, he will take the lead in guiding the choice of spectral targets and reduction of the data. He will also lead the interpretation of the earthshine spectral data from Mt. Palomar.

The BBSO earthshine team will continue to have its regularly scheduled meetings with Koonin and Yung on the Caltech campus to work on various aspects of the project. Koonin and Yung will also visit Big Bear.

Bibliography

Danjon, A., 1928. Ann. Obs. Strasbourg, 2, 165.

Danjon, A., 1954. in The Earth as a Planet ed Kuiper, p. 726, Chicago.

Dubois, J., 1947. Bull. Astron. 13, 193.

Gibson, G.G., et al., 1990, SPIE 1299, 253.

Goode, P.R., 1995, in ESA SP-376, Noordwijk, the Netherlands, p. 121.

Goode, P.R., Koonin, S.E., Qiu, J., Yurchyshyn, V., Hickey, J., Chu, M. and Kolbe, E., 2000, Science, submitted.

Flatte, S., Koonin, S. and MacDonald, G., 1991, JSR-91-315 (McLean, VA: The MITRE Corporation).

in (Radiation Characteristics of the atmosphere and the earth's surface. Editted by K.Ya. Kondratev), 1973, (available from the US Dept. of Commerce, National Technical Information Service, Springfield, Va.).

Lean, J., 1997, Ann. Rev. Astron. Astrophys. 35, 33.

Rossow, W.B. and Lacis, A.A., 1990, J. Climate 3, 1204.

Rougier, M., 1933. Ann. Obs. Strasbourg, 2, Part 3, 203.

Stephens, G, Campbell, G. and VanderHaar, T., 1981, J. Geophys. Res. 86, 9739.

Suttles, J.T., et al., 1988, NASA Reference Publications RP-1184, v.1.

Svensmark, H. and Friis-Christensen, E., 1997, J. of Atm. and Solar-Terrest. Physics 59, 1225.